The Journal of Experimental Biology 214, 1643-1654

doi:10.1242/jeb.048702

RESEARCH ARTICLE

Bottles as models: predicting the effects of varying swimming speed and morphology on size selectivity and filtering efficiency in fishes

E. W. Misty Paig-Tran[1,*], Joseph J. Bizzarro[2], James A. Strother[3] and Adam P. Summers[1]

[1]Friday Harbor Laboratories, University of Washington, 620 University Road, Friday Harbor, WA 98250, USA, [2]School of Aquatic and Fishery Sciences, University of Washington, Box 355020, Seattle, WA 98195-5020, USA and [3]University of California Irvine, 321 Steinhaus, Irvine, CA 92697, USA

*Author for correspondence (mpaig@u.washington.edu)

Accepted 30 January 2011

SUMMARY

We created physical models based on the morphology of ram suspension-feeding fishes to better understand the roles morphology and swimming speed play in particle retention, size selectivity and filtration efficiency during feeding events. We varied the buccal length, flow speed and architecture of the gills slits, including the number, size, orientation and pore size/permeability, in our models. Models were placed in a recirculating flow tank with slightly negatively buoyant plankton-like particles (~20–2000 μm) collected at the simulated esophagus and gill rakers to locate the highest density of particle accumulation. Particles were captured through sieve filtration, direct interception and inertial impaction. Changing the number of gill slits resulted in a change in the filtration mechanism of particles from a bimodal filter, with very small (≤50 μm) and very large (>1000 μm) particles collected, to a filter that captured medium-sized particles (101–1000 μm). The number of particles collected on the gill rakers increased with flow speed and skewed the size distribution towards smaller particles (51–500 μm). Small pore sizes (105 and 200 μm mesh size) had the highest filtration efficiencies, presumably because sieve filtration played a significant role. We used our model to make predictions about the filtering capacity and efficiency of neonatal whale sharks. These results suggest that the filtration mechanics of suspension feeding are closely linked to an animal's swimming speed and the structural design of the buccal cavity and gill slits.

Supplementary material available online at http://jeb.biologists.org/cgi/content/full/214/10/1643/DC1

Key words: physical model, ram filter feeding, *Rhincodon typus*, filtration efficiency, feeding selectivity.

INTRODUCTION

Filter-feeding elasmobranchs are a highly migratory and large-bodied group of fishes; these combined factors make it difficult to investigate their prey capture mechanisms in a laboratory setting or *in situ*. This type of information is important, however, because the size and type of prey that are filtered are often a determinant of distribution in these poorly known fishes (Sims and Quayle, 1998; Sims, 1999). Furthermore, prey capture and food preference in pelagic elasmobranchs represent foundational data for models that predict migratory patterns and are used to assess and maintain well-managed fisheries stocks, especially in areas where these species are harvested heavily with little regulation (Colman, 1997; Dewar, 2002; Stevens, 2007; Dewar et al., 2008).

Filter-feeding fishes consume vast numbers of tiny (5–3000 μm) prey by passing immense quantities of water through their oropharyngeal cavity (Sanderson et al., 1994; Cheer et al., 2001; Friedland et al., 2006; Smith and Sanderson, 2007). The mechanics of cartilaginous filtration are likely similar to that of smaller ram filter-feeding fishes: swimming forward with an open mouth, ingesting food particles and expelling water out of the gill openings. Food particles may be trapped on gill rakers and transported to the esophagus. Alternatively, food particles might be entrained and concentrated without ever contacting the gill rakers. Using invertebrate filter feeders as a model system, Rubenstein and Koehl (Rubenstein and Koehl, 1977) and later LaBarbera (LaBarbera, 1984) and Shimeta and Jumars (Shimeta and Jumars, 1991) described five basic mechanisms by which particles ranging in size from 10^{-7} to 10^{-1} cm can be passively intercepted by a fibrous biological filter: (1) sieve filtration, (2) direct interception, (3) inertial impaction, (4) gravitational deposition and (5) diffusion deposition.

In sieve filtration, particles that are larger than the pore size of the filter cannot pass through the mesh and are retained, whereas particles smaller than the pore size pass through (Fig. 1A) (LaBarbera, 1984). In industrial dead-end sieving, the filtering medium is positioned to lay perpendicular to the fluid streamlines, causing particle deposition to occur either along the filter's surface or as the fluid moves through the filtering element (Sibanda et al., 2001). It had been assumed that filtering fishes sieve their planktonic prey, but this notion was refuted by a gut content study showing prey sizes smaller than the distance between gill rakers (Langeland and Nøst, 1995). In the remaining mechanisms of filtration, particles smaller than the filter's pore size are captured by direct contact with the filtering element (LaBarbera, 1984; Shimeta and Jumars, 1991). Direct interception is the most common form of particle capture among marine invertebrate filter feeders (Rubenstein and Koehl, 1977). This occurs when a neutrally buoyant particle following a streamline comes within one particle radius of a filtering fiber, where it adheres to mucus or some other adhesive surface. Conversely, in

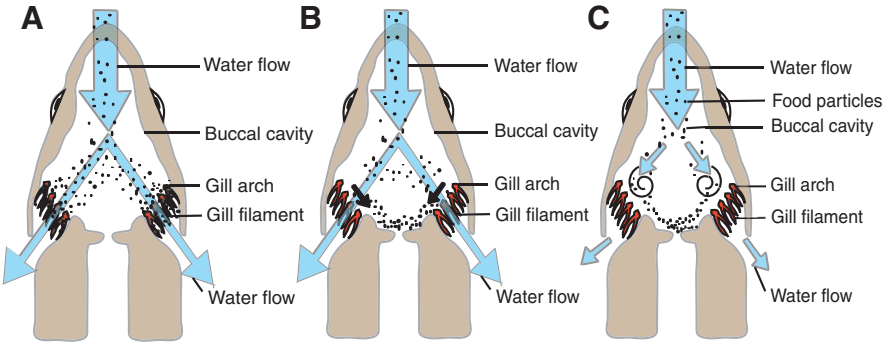

Fig. 1. Mechanics of particle filtration for three types of filter-feeding bony fishes. (A) Sieve filtration. Particles of all sizes adhere to the gill rakers by contacting the filtering element. (B) Cross-flow filtration. Particles encounter strong shearing forces that push particles towards the esophagus. (C) Vortex filtration near the gill openings. Particles accumulate at the esophagus by centrifugal forces as water exits out of the operculum.

inertial impaction, a sharp turn in the fluid streamline causes a negatively buoyant particle to leave the streamline and impact a filtering surface (Rubenstein and Koehl, 1977). Gravitational deposition is similar to inertial impaction except that particles are not separated from the fluid by a sharp acceleration of the streamline, but rather by a constant gravitational force (Rubenstein and Koehl, 1977; LaBarbera, 1984; Shimeta and Jumars, 1991). Finally, in diffusion deposition, very small particles deviate from the streamlines because of random Brownian motion (Rubenstein and Koehl, 1977; LaBarbera, 1984; Shimeta and Jumars, 1991). This method captures particles smaller than those that are important for ram filter-feeding organisms.

Fishes filter feed at higher Reynolds numbers than invertebrates, and two additional methods should be considered: cross-flow filtration and vortex filtration. Industrial cross-flow filtration takes advantage of the shear generated by fluid flow parallel to the surface of a filter to clear the filter mesh of trapped particles and concentrate them at the end of the filter chamber (Bott et al., 2000; Sibanda et al., 2001). This has been hypothesized to work in some filter-feeding fishes when ingested food particles do not contact the gill rakers; instead, they travel parallel to the surface, eventually concentrating near the esophageal opening (Fig. 1B) (Brainerd, 2001; Sanderson et al., 2001; Callan and Sanderson, 2003). The final method of filtration that should be considered is vortex or hydrocyclone filtration (Fig. 1C). In this case, water and food particles would enter through the mouth into a bilaterally symmetrical vortex near the internal gill openings. Water would then exit out the gill slits and food particles would be collected near the esophagus or resuspended inside the buccal cavity, increasing the chances of collision with sticky surfaces near the esophageal opening. The mechanics behind this are best appreciated by an analogy to a common household vacuum. Some bagless models use vortex filtration where dirt-laden air is entrained in a vortical flow inside a cylindrical or conical chamber. The rotation of the fluid establishes a radial pressure gradient exactly sufficient to maintain a circular trajectory for a neutrally buoyant particle. However, this pressure gradient is insufficient to maintain a circular trajectory for negatively buoyant particles, which subsequently accumulate near the periphery (Trakumas et al., 2001). The densest and largest particles will be expelled early in the cyclone whereas the smaller and less dense particles will only be expelled with a narrowing vortex. The clean air then passes back through the center of the vortex and exits out the top of the cylinder.

We faced an interesting challenge – a range of possible filtration types with associated differences in prey capture mechanisms and efficiencies and a set of fishes that is both morphologically diverse and experimentally intractable. We suggest that simple physical models are the best routes to investigate an initial set of predictions about filtration efficiency and prey size selectivity. We therefore tested a model of the open mouth of a ram-filtering fish that samples particles both from a simulated esophagus and from a set of simulated gill slits equipped with gill rakers. We expected this model to give us qualitative insight into the effect of variation in morphological (e.g. gill slit number, size, angle and buccal length) and physiological (e.g. flow velocity) parameters on efficiency and selectivity.

Our goals in this study were to: (1) show that a simplistic physical model loosely based on a filter-feeding elasmobranch allowed us to measure trends in size selectivity and efficiency of particle capture; (2) determine the effect of changing swimming speed on the size distribution of captured particles; (3) determine the effect of morphological variation, including variation in gill slit number, gill slit orientation, gill permeability and buccal depth, on the size distribution of captured particles; (4) test the relative importance of the gill rakers and the esophagus in particle capture; and (5) use measurements and inferred swimming speeds from neonatal whale sharks to predict their ability to filter different sized prey items from the water column.

MATERIALS AND METHODS

Anatomy of the filtration system

Four neonatal whale sharks, *Rhincodon typus* (Smith 1828), were obtained from the Marine Vertebrate Collection at Scripps Institute of Oceanography (La Jolla, CA, USA). We measured each shark's total length (TL), fork length (FL), gill width when the gill opening was fully stretched, gill height, distance from the opening of one gill slit to the next, mouth height, mouth width and total distance from the leading edge of the mouth to the esophageal sphincter (orophanyngeal distance). We also measured the distance between the gill rakers, which we refer to as pore size. Gill width, gill height and distance between gills were expressed in order from gill 1 (closest to the mouth) to gill 5. The four neonatal whale sharks ranged in size from 533–591 mm TL and 439–468 mm FL (Table 1). It is important to note that the simplistic model is only loosely based on the anatomy of the neonatal whale sharks. The model's purpose is to understand how differing fish morphologies affect filtration efficiency and size selectivity. To accurately predict the prey of neonatal whale sharks, we would suggest using a model that more closely resembles this fish, e.g. a three-dimensional rapid prototyped model based on computed tomography scans.

Predicting swimming speed

To determine the mean swimming speed of neonatal whale sharks, we compared log-transformed length data from measured whale sharks (TL or FL) with log-transformed mean swimming speeds of both sharks and bony fishes compiled from published literature (see

Table 1. Anatomical measurements of four neonatal whale sharks (*Rhincodon typus*)

Specimen	Total length (mm)	Fork length (mm)	Gill width (mm)	Gill height (mm)	Distance between gill slits (mm)	Mouth height (mm)	Mouth width (mm)	Oropharyngeal distance (mm)
1	561	445	–	42, 45, 50, 51, 42	8, 10, 8, 7	33*	92	105
2	566	468	**6, 8, 5, 3, 2	36, 40, 41, 39, 32	14, 12, 10, 10	26	72	83
3	591	439	27, 28, 28, 25, 22	41, 46, 48, 40, 36	17, 15, 17, 9	15	82	108
4	533	447	17, 19, 19, 15, 13	36, 37, 39, 35, 29	10, 11, 9, 8	16	69	100

Gill width and gill height measurements are listed in order from gill 1 (closest to mouth) to gill 5.
*, Not fully extended when measured; **, not fully opened when measured.

supplementary material Table S1). The relationship between fish length and swimming speed was analyzed using linear regression (SPSS Statistics 16, IBM, Somers, NY, USA). It is important to note that adult filter-feeding sharks appear to swim at slower speeds [<0.1 body lengths (BL) s^{-1}] than other sharks and bony fishes. However, because swimming speeds have never been measured on neonatal whale sharks, we based our predictions on the relationship between an organism's size and known swimming speeds, not on those of adult filter-feeding sharks.

Filtration models

To estimate the effects on filtration efficiency from individual parameters, we constructed models of a ram suspension-feeding fish roughly based on morphological measurements of neonatal whale sharks (photos of ram feeding adult whale sharks are available in supplementary material Figs S1–S3). Our simple cylindrical models were created from 1 l soda bottles with the bottom cut off so that the mouth of our model had an 8.5 cm diameter. A cylindrical model was selected over a conical model based on both our observations of filter-feeding adult whale sharks in the Yucatan and observations of ram filter-feeding bony fishes by Cheer et al. (Cheer et al., 2001), who noted that gill arch abduction during ram feeding resulted in the oral cavity of the fish becoming more cylindrical in appearance. The length of the bottles was 23.0 cm including the neck of the bottle and 19.5 cm without the neck. We plugged the neck of the bottle with a rubber stopper to simulate a closed esophageal sphincter. A 4 mm diameter tube was inserted through the stopper so the leading edge was exposed to the posterior buccal cavity. The end of the tubing outside of the bottle was connected to a peristaltic pump to simulate particle ingestion through the tubing at a constant rate of 8.2 ml min^{-1}. Gill openings were cut with polyethylene mesh of various sizes to simulate different gill resistivities.

For the experiments we started with a standard model that was similar to the morphology measured for neonatal whale sharks, with a few adjustments: four gill openings [which is intermediate between bony fishes (with a singular opercular opening and five gill slits with four gill arches on each side of the pharynx) (Harder, 1975) and the elasmobranches (with five to seven gill slits and typically five gill arches on each side of the pharynx) (Butler, 1999)], 90 deg gill orientation to the midline of the bottle (Cheer et al., 2001), 0.5 cm gill width, 4.5 cm gill height, a buccal cavity (mouth to final gill opening) 19.5 or 23 cm from mouth to esophagus, 1000 μm mesh net covering the gill openings (measured in neonatal whale sharks), and 45 cm s^{-1} flow speed. We then systematically manipulated gill number (one, two, three, four and five gill openings), as there is some evidence that elasmobranch parabranchial chambers receive varying amounts of water flow and have differing levels of oxygen extraction (Piiper and Schumann, 1967; Ballintijn, 1972; Summers and Ferry-Graham, 2001), gill orientation [0 and 55 deg orientation to the midline, similar to Cheer et al. (Cheer et al., 2001)] and permeability (no mesh, 105, 200 and 2000 μm to represent differing pore sizes of fishes). The 105 and 200 μm mesh sizes were similar to the width between rakers measured in smaller teleosts [e.g. herring (Gibson, 1988), singidia tilapia (Goodrich et al., 2000), and Japanese anchovy, Pacific round herring and Japanese jack mackerel (Tanaka et al., 2006)], and the larger mesh size (1000 μm) was similar to those measured from neonatal whale sharks (Motta et al., 2010). Gill size was increased to 1.5 cm width, representing the enlarged gill slits of the basking shark, buccal length was decreased (to 15 cm total, 12 cm buccal) to test for differences in ontogeny, and flow speed (fish swimming speed) was increased to 60 cm s^{-1} for each gill number variation.

Adjusting each feeding parameter separately allowed us to test our initial hypotheses about how differing morphologies affect filtering performance. First, in all treatments, we hypothesized that the majority of particles collected would be larger than the mesh size if direct interception is the primary mechanism of filtration, and a mixture of particle sizes if other mechanisms of filtration are occurring. Second, we hypothesized that, if cross-flow filtration is occurring, the majority of particles would be trapped close to or inside the esophagus. Third, we hypothesized that increasing the swimming speed should increase the filtration efficiency because more particles will come into contact with the filtering elements if some form of direct interception or inertial impaction is occurring. Similarly, the filtration efficiency should also increase with smaller mesh sizes. Fourth, we hypothesized that the slanted gill orientation would affect the flow through the buccal cavity and, similarly, may alter the mechanism of filtration by creating a vortex near the third or fourth gill slit. Fifth, we hypothesized that reducing the buccal length would result in higher flow through the buccal cavity, creating additional turbulence near the gill slits. This additional turbulence may result in longer periods of particle resuspension, reducing the number of particles that come into contact with the filtering medium and hence reducing the filtering efficiency. Finally, we hypothesized that increasing the gill slit size would increase the surface area for filtration, resulting in increased filtration efficiency.

The models were based on the morphology of the neonatal whale sharks with a few key exceptions. The gill widths were measured by adjusting the gill flaps so that they were fully open during measurements. However, in all but one trial, we adjusted our bottle's parameters so that only a portion of the flap would be open during feeding, as it is unlikely that these gill coverings are fully stretched during a feeding event. Mouth height and width remained fixed in all models. It is also important to note that filter-feeding sharks have a variety of mouth shapes and heights. We chose a cylindrical version to model, but adjustments to the mouth morphology may lead to differences in size selectivity and filtration efficiency.

Filtration experiments

Experiments were carried out in an 80×28×28cm recirculating freshwater flow tank with a 42×28×28 cm working area and 260 l total volume. The model was secured in the center of the tank using

fishing line, which was anchored above the tank. To mimic plankton, we milled 20 mm poly(methylmethacrylate) cylinders to produce slightly negatively buoyant, irregularly shaped particles (density 1.14 g cm^{-3}) ranging in size from 20 to 2000 μm. Density for marine copepods has been estimated at 1.027 to 1.047 g cm^{-3} (Knutsen et al., 2001). The size classes chosen were based on the series of meshes used during the experiments (e.g. 100, 200, 1000 and 2000 μm). These size classes also coordinate with those typically seen in plankton assemblages (e.g. >1000 μm are the largest zooplankton, 501–1000 μm large zooplankton and ichthyoplankton, 101–500 μm microcrustaceans, 51–100 μm net phytoplankton and small zooplankton, and 10–50 μm nanoplankton) (Moloney and Field, 1991). The use of non-spherical particles does cause some complications in understanding how the particles react within the flow (e.g. their orientation); however, we believe that using particles similar to those collected during an actual feeding event gives us a better understanding of how plankton would be captured along the gill rakers or at the esophagus. Sixty grams of particles were added to the flow tank and allowed to circulate for 1 h prior to experimentation to approximate equal distributions throughout the tank. The initial seeding density was collected and measured so that we could compare the particle size distributions in individual experiments with the total size distribution within the tank. The tank was only seeded a single time during these experiments because the particles collected during all 64 experiments comprised less than 3% of the total particles within the flume.

The model was oriented with the gape facing into the flow, mimicking the conditions experienced by a ram filter-feeding fish during a feeding event (Fig. 2). Particles moved through the buccal cavity and were collected either on the gill rakers or inside the esophagus. Esophageal particles were pumped through the tube and were captured in an external flask. The bottles remained in the flow for a total of 3 min, a period chosen because there was very little clogging of any mesh size during this brief exposure. During elasmobranch feeding events, raker clogging is likely prevented by periodic swallowing of the collected plankton. At the end of the experimental run, the leading edge of the bottle was covered and particles that remained on the mesh and those contained in the external flask were collected. Each experiment was replicated four times for a total of 64 experiments.

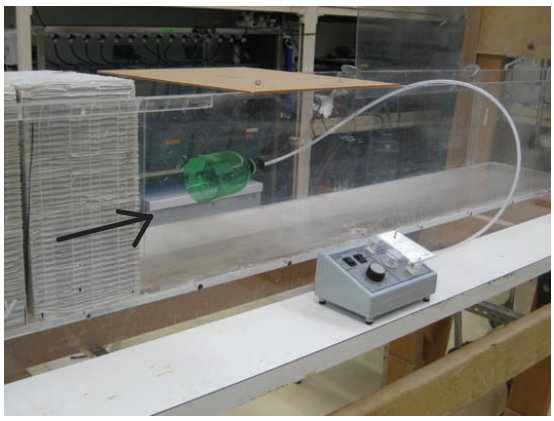

Fig. 2. Model inserted into the flume and attached to a peristaltic pump, which functioned as an esophagus during trials. Water and particles move past a series of flow straighteners; the direction of movement is illustrated by the arrow.

Permeability measurements

Permeability measurements of the entire gill structures were performed on intact neonatal whale sharks. Each shark was placed in a 153 l ice chest filled with distilled water. Water was pumped out from the ice chest at a constant flow rate of 114 ml s^{-1} with a Flojet Model 2100–953–115 pump (ITT Corporation, Santa Ana, CA, USA) into a 4.41 l cylindrical (441 cm^3) tank, which functioned as a manometer. Water flowed gravimetrically from the cylindrical tank into the neonatal shark's buccal cavity using 1.4 cm diameter plastic tubing. The tubing was inserted into a mask that sealed within the shark's mouth (the mask was constructed from closed-cell polyurethane foam for larger individuals and molded silginate for small individuals) so that the resistance of the gill openings could be estimated by the change in water column height (pressure) in the cylindrical tank. We calculated the resistance of a neonatal whale shark's buccal cavity using the equation:

$$R = \frac{\Delta P}{Q}\,, \tag{1}$$

where R is the resistance through the gill structure, ΔP is the change in pressure estimated by measuring the change in water height of the manometer when the shark was attached to the tubing, and Q is the flow rate. These measurements helped us to determine whether the entire gill structure (including the gill filaments which were ignored during these trials) had a high level of resistance to flow. The change in pressure (ΔP) was calculated as:

$$\Delta P = \rho \boldsymbol{g} h\,, \tag{2}$$

where ρ is the density of water, $\boldsymbol{g}$ is gravity and h is the mean change in height of the manometer. This equation allowed us to estimate the permeability of the gill structures in preserved neonatal whale sharks (N=3, as one shark could not be measured) within an order of magnitude. We compared the whale shark's permeability measurements with those measured from neonatal specimens of three additional filter-feeding elasmobranchs, *Mobula munkiana* (N=2) and *M. japonica* (N=1).

Reynold's flow (Re), the ratio of inertial to viscous forces, is an important component when attempting to quantify the effect of a filtering element on the flow around it (Shimeta and Jumars, 1991). Reynolds conditions at the level of the gill slits were calculated using the standard equation:

$$Re = QL / \nu A\,, \tag{3}$$

where Q is the flow at the level of the gill slits, L is the permeability of the mesh rakers, ν is the kinematic viscosity and A is the total area of gill openings.

Data analysis

We assessed the initial distribution of particle sizes by homogenizing the milled (seeding) particles, collecting a large subsample (N=10,395 particles) and determining its size distribution. Following trials, we also subsampled from the particles collected on the gill rakers. All esophageal particles were measured because of the relatively small number collected there. We recognize that errors in plankton subsampling are common (van Guelpen et al., 1982); however, these errors are reduced by increasing sampling size. Our seeding subsampling is based on over 10,000 particles for a total of six separate subsampling events. Experimental trial data were based on five separate subsampling events from each replication (or 20 subsampling events). Trial run order was chosen haphazardly except that some 45 cm s^{-1} trials were run prior to 60 cm s^{-1} trials and some were run after.

To ensure that particle distributions within the flume remained similar over time (e.g. to ensure that larger particles did not settle out of the water column), we performed a separate sampling experiment. Once again we milled 60 g of particles, subsampled from the initial seeding density, allowed the particles to circulate within the running flume at 45 cm s^{-1} for 1 h prior to subsampling, and then subsampled particles for 1 min at 30 min intervals for a total time period of 240 min (i.e. at 0, 30, 60, 90, 120, 150, 180, 210 and 240 min) using a 105 µm net. Following the same sampling techniques as the experiments, we compared the subsamples with the initial seeding density distributions. We compared the distributions, first excluding particles <100 µm and again excluding <50 µm to reduce errors from sampling with a net that is larger than two of our particle size categories and because we are primarily interested in understanding how the distributions of the larger zooplankton change, not the distributions of nanoplankton and phytoplankton, which are not the food sources being targeted. The different size classes of plankton were classified as follows: 1–50 µm=very small, 51–100 µm=small, 101–500 µm=intermediate, 501–1000 µm=large and >1000 µm=very large. We performed a weighted linear regression of the combined percentage of intermediate, large and very large plankton collected during subsampling events over 240 min.

All subsamples were collected, mounted on slides so that the particles didn't touch and analyzed for size distribution using a Zeiss steREO Discovery V20 microscope (Carl Zeiss Imaging Gmbh, Jena, Germany). Particles were viewed using the microscope imaging program Axio Vision (Carl Zeiss) and photographed using a Zeiss Axiocam HRC camera. Photos were then uploaded into NIH Image J software (version 1.4, http://rsbweb.nih.gov/ij/) for analysis. We measured the total area and the mean Feret's diameter for each particle in the subsamples (N=10,395) of the seeding particles and the experimental trial subsamples. Although creating a continuous scale for these particles would give us a more in-depth visualization of their actual size distribution, binning particles into size classes is an easier way to visualize trends in particle capture and to infer results by comparing the sizes of experimental particles with live plankton size classes. The color scheme for size classes will remain constant throughout all histograms (Figs 4–8).

Filtering efficiency was determined by weighing air-dried particles for each replication of the trials. Data are expressed as mean efficiencies for all four trials. The weights of the collected particles were small compared with the seeding density, so efficiency values are expressed as per mil (‰) rather than as a percentage. Filtration efficiency (E), or the percentage of weight-specific particle capture per 3 min trial, was calculated using the equation:

$$E = 1000 \times \frac{W_P}{W_S}\ , \qquad (4)$$

where W_P is the weight of the particles either at the esophagus or at the gill rakers and W_S is the calculated total weight of the seeded particles within the flume that are predicted to flow through the model's aperture. This allowed us to get a snapshot of the amount of particles (by weight) being filtered within a relatively short amount of time. Because we had such a small amount of particles collected per trial, the filtering efficiencies are expressed as total efficiency over the full 12 min. Note that filtration efficiency is used as a proxy for determining the amount of particles (by weight) collected along the gill rakers over 12 min compared with the amount of particles available in the flume. Our filtration efficiency calculation is similar to methods of industrial filtration efficiency, which is expressed as {[1–(downstream concentration/upstream concentration)]×100}. This is vastly different from filtering efficiencies expressed in live fishes (Drenner and Mummert, 1984; Garrido et al., 2007).

We predicted that changing the morphology (i.e. gill number, raker permeability, buccal length, gill-slit orientation and gill size) and/or the swimming speed of the model would affect the size distribution of particles collected along the gill rakers; therefore, we hypothesized that particle distributions collected during the experiments would not be the same as the seeding distribution. To test this hypothesis, four replicates of each version of the physical model were compared with six replicates of the initial seeding distribution for the five particle size categories. The various physical models were then compared with the basic model (four gill slits, 45 cm s^{-1} flow) in the same manner to further evaluate the effects of model alterations.

Poisson regression was used to determine whether particle distributions differed significantly between the seeding distribution and the various physical models, and between the basic physical model and the other model variants. The generalized linear model (GLM) used in comparisons was of the basic form: log(no. particles)=source×size category, and was analyzed using analysis of deviance (ANODEV) (Skalski, 1996). The process of analyzing GLMs with ANODEV is analogous to analyzing linear models with ANOVA, but more appropriate for the replicated contingency table design used in this study. The scale parameter ($MDEV_{error}$=$SS_{error}/d.f._{error}$) of the interaction term was calculated from ANODEV results to determine the amount of dispersion. For overdispersed data (scale parameter>1), F-statistics were calculated; in contrast, χ^2 statistics were considered to be more appropriate when data were underdispersed (scale parameter<1).

RESULTS

Swimming speed

Swimming speed decreased significantly with length based on the available teleost and elasmobranch data (r^2=0.59, P<0.001; Fig. 3). This relationship was best represented by the following equation: swimming speed(BL s^{-1})=18.30$x^{-0.78}$, where BL is body length. Based on these results, we predict that a neonatal whale shark of

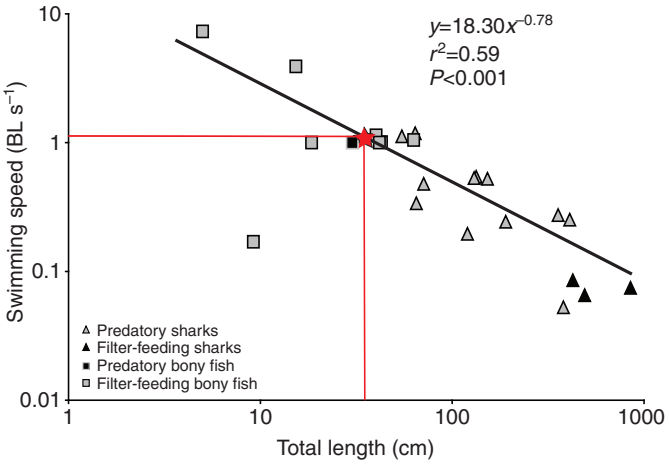

Fig. 3. Relationship between mean total length of a fish (by species) and swimming speed. Neonatal whale sharks are estimated to swim at approximately 1 body length (BL) s^{-1} (45–60 cm s^{-1}; red star). The teleost outlier is *Silurus glanis*, a species of river catfish that is a sluggish swimmer. References for data can be found in supplemental material Table S1.

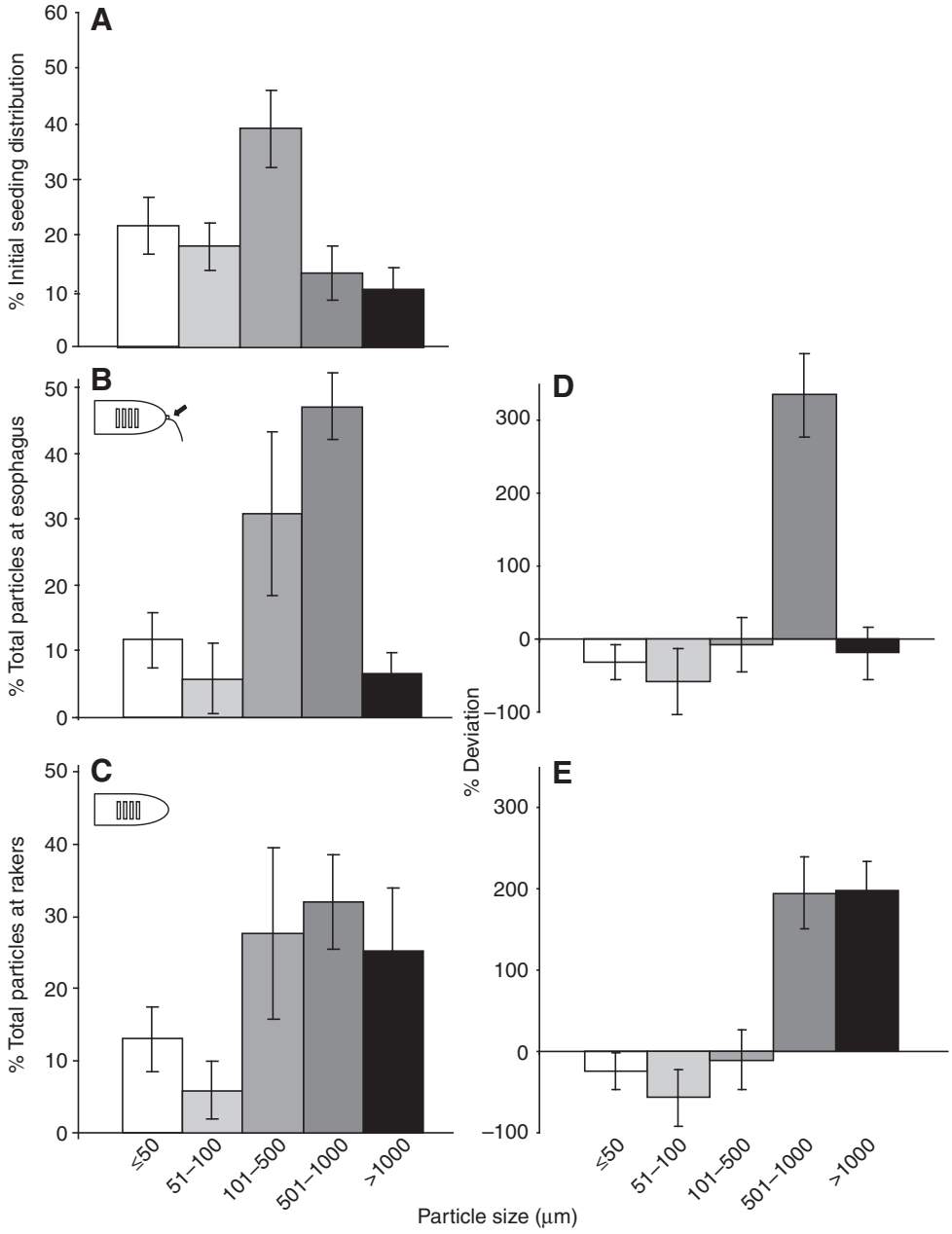

Fig. 4. Comparison of the standard model with seeding density. (A) Initial seeding density of particles in the flume (N=10,395). (B,C) Distributions of particles collected at the esophagus and the gill rakers, respectively. (D,E) Percentage deviation of particles from the initial seeding density collected at the esophagus (N=135, E=0.006‰) and the gill rakers (N=263, E=0.56‰), respectively. Only mean percentage deviation is shown from this point forward. E, mean filtering efficiency; N, number of particles subsampled.

approximately 50–60 cm TL swims at approximately 1 BL s^{-1}, or 45–56 cm s^{-1}.

Flume seeding

We found that intermediate, large and very large particles remained suspended in the water column throughout the full 240 min trials; therefore particle settling was negligible (r^2=0.01, P=0.79) (see supplemental material Fig. S4). Our initial seeding distribution of particle sizes in the recirculating flume was primarily composed of intermediate particles between 101 and 500 μm in diameter (Fig. 4A). Seeding distributions are represented as mean (±s.d.) percentages of the total particles that were subsampled (N=10,395) from the 60 g of seeding particles.

Standard model

Our standard model collected particles in the intermediate to large size classes (101–1000 μm) at the esophagus and large particles (501–1000 μm) at the gill rakers (Fig. 4B,C, respectively). The Re at the level of the filtering elements was calculated to be 1.4×10^5. Compared with our seeding density, there was a threefold increase in large particles (501–1000 μm) collected at the esophagus (Fig. 4D) and a twofold increase in large particles collected at the gill rakers (Fig. 4E), even though there were almost twice as many 101–500 μm particles seeded in the tank. Comparisons of the seeding distribution treatment with the standard model for all five seeding categories showed that the distribution of particles collected at the gill rakers was significantly different from the initial seeding morphology; i.e. there was a significant increase in large and very large particles ($F_{4,40}$=4.71, P<0.001). Specifically, there was a twofold increase in very large (>1000 μm) particles collected along the rakers. The filtration efficiency for esophageal particles was very low (total particles collected, N=135, E=0.006‰) and much higher at the rakers (E=0.56‰). Because there was very little filtration occurring in the esophagus, we will

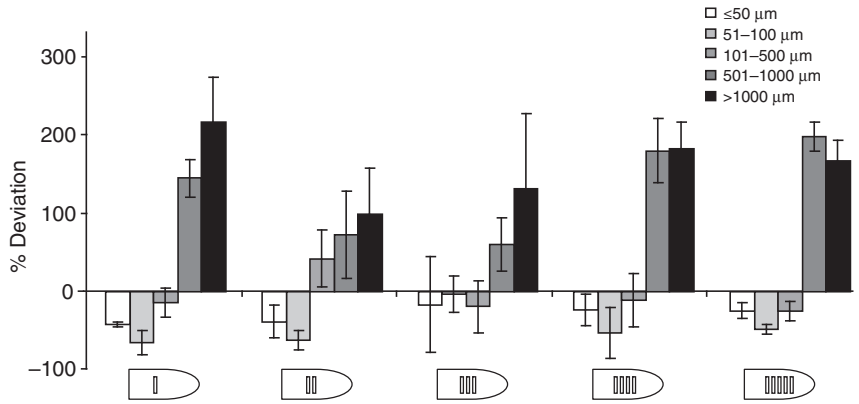

Fig. 5. Percentage deviation from the seeding density (±s.d.) in particles collected at the gill rakers at 45 cm s^{-1} with differing numbers of gill slits: one gill (N=287, E=0.34‰), two gills (N=592, E=0.25‰), three gills (N=288, E=0.11‰), four gills (N=263, E=0.56‰) and five gills (N=430, E=0.52‰). Data are means ± s.d.

focus on the particle capture at the gill rakers. Therefore, we conclude that our model did not evenly collect particles from the tank; instead, selective filtering occurred.

Gill number

The majority of particles collected in the esophagus for all permutations of the model were in the 101–1000 μm size range, as in the control model. Few particles were 'swallowed' at the esophagus in any of the five treatments (N=19–226 total particles over four replicates) and the mean total efficiencies over all five variations were extremely low (E<0.01‰ total). We did observe a very slow-moving esophageal vortex during the trials that increased in speed as we increased the number of gill openings. Additionally, in the four- and five-gill trials, we noticed an increase in the number of particles collected in the esophagus (N>100) compared with the one-, two- and three-gill treatments. When we increased the experimental number of gill slits to four or five, there was turbulence near the esophageal opening; however, we could not determine whether it was a single vortex or a pair of vortices. This turbulence was rather slow moving during the one- and two-gill trials and appeared to increase in speed in the trials with higher numbers of gill slits.

Examination of the particles collected at the gill rakers showed a shift in particle distribution from the initial seeding distribution (Fig. 5). Re for one, two, three, four and five gills were 5.6×10^5, 2.8×10^5, 1.9×10^5, 1.4×10^5 and 1.1×10^5, respectively. In the one-gill model, the particles collected on the rakers were mostly small (51–100 μm) or large to very large (>500 μm) and the distribution was statistically different from that of the seeding distribution ($F_{4,40}$=8.16, P=0.003). As we increased the number of gill openings, the size distribution of particles collected shifted to large to very large particles (>500 μm) and all permutations except three gills were significantly different from the seeding distribution (two gills, $F_{4,40}$=3.67, P=0.01; three gills, $F_{4,40}$=2.40, P=0.07; four gills, $F_{4,40}$=4.71, P=0.003; and five gills, $F_{4,40}$=10.63, P<0.001). The physical model transitioned from behaving as a bimodal-type filter that collects particles in two narrow size ranges to an intermediate-type filtration system that collects particles in a much broader size range. Although our method precluded a quantitative examination of the filtering performed at each gill slit, certain trends in particle deposition were evident. During the two-gill trials, more particles were caught in the first gill slit (the opening closest to the mouth of the model) than in the second, whereas in the three-gill trials, particles were captured primarily at the third gill slit. Particles appeared evenly distributed across all slits in the four- and five-gill trials.

Throughout all trials we collected fewer very small (≤50 μm) and intermediate particles (101–500 μm) compared with the seeding distribution; however, each trial also collected more large and very large particles (>500 μm) than expected. Filtration efficiency decreased during the first three trials and then increased during the four- and five-gill trials. The total efficiencies from each trial were as follows: one gill, 0.34‰; two gills, 0.25‰; three gills, 0.11‰; four gills, 0.56‰; and five gills, 0.52‰.

Comparisons of the standard model with the one-, two-, three- and five-gill trials showed that the distributions from all but the two-gill permutation were significantly different from the standard model (one gill, $F_{4,30}$=6.71, P=0.001; two gills, $F_{4,30}$=1.65, P=0.19; three gills, $F_{4,30}$=7.02, P=0.004; five gills, d.f.=4, χ^2=46.28, P<0.001). The distributions of small and intermediate particles were similar to those in the standard model except there was a 20% increase in intermediate particles in the two-gill permutation. The proportion of large particles was approximately 11% less than the standard model in the two- and three-gill trials.

Change in speed

The total number of particles collected at the esophagus and at the gill rakers was more numerous at a flow speed of 60 cm s^{-1}. There was a more even distribution of particle sizes both at the esophagus and at the gill rakers (Fig. 6) compared with the standard model. Re at 60 cm s^{-1} were as follows for one-, two-, three-, four- and five-gill trials: 7.4×10^5, 3.7×10^5, 2.5×10^5, 1.9×10^5 and 1.5×10^5, respectively. During these trials, increasing the number of gill slits to five resulted in smaller particles collected on the rakers and, in all but the five-gill trials, resulted in distributions that were significantly different from those of the seeding density (one gill, d.f.=4, χ^2=6.60, P<0.001; two gills, d.f.=4, χ^2=5.74, P<0.001; three gills, $F_{4,40}$=8.99, P<0.001; four gills, $F_{4,40}$=5.71, P<0.001, five gills, $F_{4,40}$=1.97, P=0.88). Trials with fewer gill openings collected particles primarily in the intermediate to large size range (101–1000 μm). We noticed the same basic trends in the 45 cm s^{-1} trials (e.g. one-gill trials picked up a lot of particles within 10 to 20 s) and once again the speed of the esophageal vortex or vortices was much faster in the four- and five-gill permutations. More large and very large particles were collected compared with the seeding distribution.

At the higher speed, filtering efficiency did not increase with the number of gill slits. The 60 cm s^{-1} efficiencies were all lower than the corresponding 45 cm s^{-1} treatments (one gill, E=0.16‰; two gills, E=0.04‰; three gills, E=0.02‰; four gills, E=0.05‰; five gills, E=0.04‰).

The distribution of particles from all of the increased speed trials except the one-gill trial differed significantly from the standard

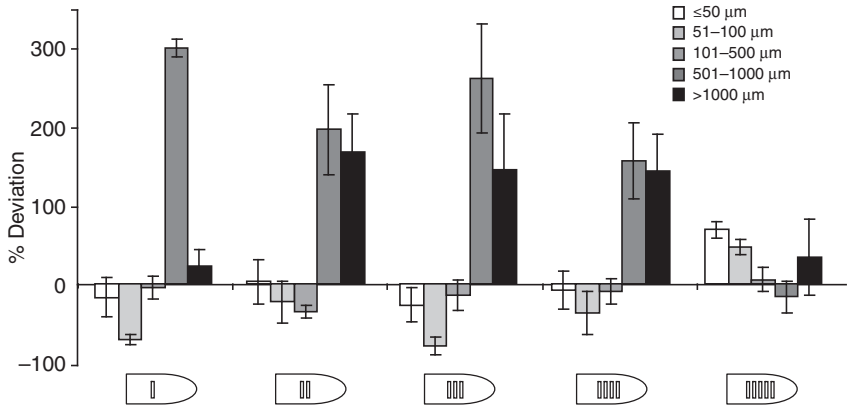

Fig. 6. Percentage deviation from the seeding density (±s.d.) in particles collected at the gill rakers at an increased flow speed of 60 cm s^{-1} with differing numbers of gill slits: one gill (N=229, E=0.16‰), two gills (N=303, E=0.04‰), three gills (N=315, E=0.02‰), four gills (N=538, E=0.05‰) and five gills (N=1738, E=0.04‰). Data are means ± s.d.

model (one gill, $F_{4,30}$=2.63, P=0.621; two gills, $F_{4,30}$=31.01, P<0.001; three gills, $F_{4,30}$=3.75, P=0.01; four gills, $F_{4,30}$=5.65, P=0.002; five gills, $F_{4,30}$=16.69, P<0.001). There was an approximately 10% increase in very small particles during the five-gill trial compared with the standard model, and the five-gill trials also collected a higher proportion of small particles (14%) compared with the standard model. There was also a higher proportion of the large particles collected in the one-gill trials (~11%) compared with the standard model. Finally, there was a smaller proportion of very large particles collected in each of the 60 cm s^{-1} trials, with the largest difference in the one-gill trials (~14% less than the standard).

Gill orientation

Adjusting the gill orientation did not change the distribution of particles collected at the esophagus; however, there was a shift from a band-pass-type filter in the 90 deg orientation to a notch-type filter in the 55 deg orientation at the gill rakers (Fig. 7A), although the *Re* did not change. Particles collected in the 55 deg orientation were primarily very small (<50 μm) or very large (>1000 μm) and the raker distributions were significantly different from the seeding distributions ($F_{4,40}$=6.04, P<0.001). There was no noticeable increase in turbulence near the gill slits with this change in gill orientation; however, particle capture occurred primarily along the lower portion of the third and fourth gill openings. The total filtration efficiency for the 55 deg trials (0.12‰) was much lower than for the 90 deg trials (0.56‰). The distribution of particles in the 55 deg orientation model differed significantly from the standard model ($F_{4,30}$=17.33, P<0.001). There was an increase in very small particles collected (~18%) and a decrease in the proportion of intermediate and large particles (~10 and 21% decrease, respectively) compared with the standard morphology, resulting in a more even distribution of particles.

Table 2. Calculated extrinsic resistance through the buccal cavity of three neonatal whale sharks compared with other filter-feeding elasmobranchs

Specimen	Change in pressure (Pa)	Resistance (Pa ml^{-1} s^{-1})
Rhincodon typus 2	106.19	0.93±0.05
Rhincodon typus 3	718.86	6.31±0.30
Rhincodon typus 4	449.89	3.90±0.37
Mobula munkiana 1	782.35	6.86±0.42
Mobula munkiana 2	261.62	2.29±0.21
Mobula japonica 3	113.29	0.99±0.006

Resistance data are means ± s.e.m.

Oropharyngeal cavity

A shortened oropharyngeal cavity did not affect the size distribution of particles collected in the esophagus. Particles collected along the rakers were primarily very small (≤50 μm) or large to very large (>501 μm), and the distribution was significantly different from the seeding density distribution ($F_{4,40}$=4.28, P<0.001) (Fig. 7B). The shortened morphology resulted in an increased vorticity inside the buccal cavity, as expected; however, we did not predict that there would also be an increased rate of particle ejection out of the leading edge of the model. The total filtering efficiency (0.12‰) was much lower relative to that in the longer buccal cavity model (0.56‰). The distribution of particles in the shortened buccal model differed significantly from the standard model ($F_{4,30}$=4.72, P=0.004). There was a slight increase in the proportion of very small particles (~8%) compared with the standard model and the total distribution of particles collected was more even across size classes.

Increased gill width

An increased gill width decreased the relative contribution of very small particles that were collected in the esophagus from 12 to 3%. The particles collected at the gill rakers were primarily very small to small (≤100 μm) or very large (>1000 μm) and the particle distributions along the rakers were significantly different from the initial seeding distributions ($F_{4,40}$=3.57, P<0.001) (Fig. 7C). *Re* were 4.7×10^4 in all trials. Filtration efficiency did not increase with increased gill size (E=0.21‰). The distribution of particles in the increased gill model differed significantly from the standard model ($F_{4,30}$=14.09, P<0.001). There was an increase in the proportion of small particles (~25%) and a decrease in intermediate and large particles (~15 and 22%, respectively) compared with the standard model.

Permeability

Adjustments to gill raker permeability did not affect the distribution of particles collected at the esophagus. Particles collected at the esophagus were in the large size range (501–1000 μm) during all trials. The distributions of particles collected in the esophagus using the 105 and 200 μm mesh were similar to those collected using the 1000 μm mesh (mostly 100–1000 μm particles). The amount of particles collected at the esophagus was low compared with that collected along the gill rakers, ranging from a total of 10 particles collected over four replicates in the absence of gill rakers to a total of 135 particles collected over four replicates in the 1000 μm mesh trials. During the 1000 μm mesh trials we noticed the presence of turbulence near the esophageal opening; however, we could not determine whether this was a bilaterally symmetric vortex or a single esophageal vortex.

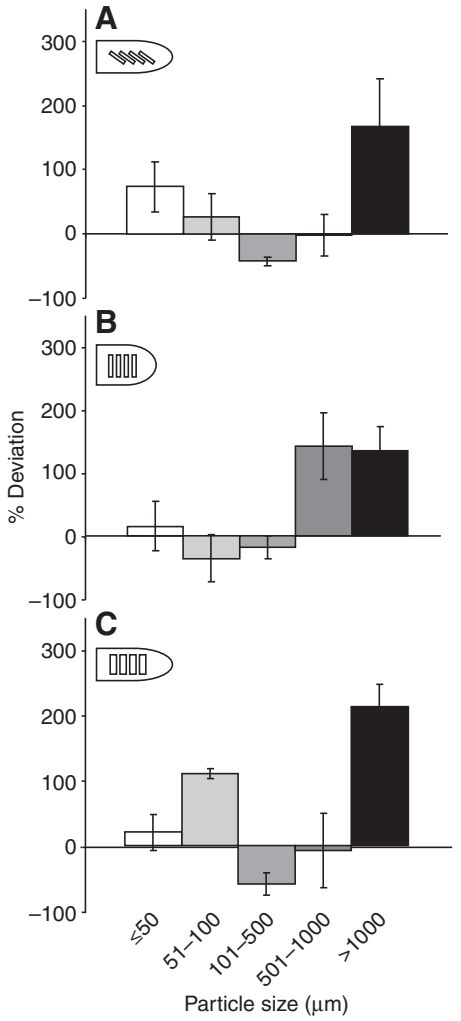

Fig. 7. Percentage deviation from the seeding distribution for (A) 55 deg gill orientation (N=510, E=0.12‰), (B) shortened buccal cavity (N=364, E=0.12‰) and (C) enlarged gill slits (N=510, E=0.21‰). Data are means ± s.d.

Particles collected along the gill rakers at increasing pore sizes displayed a shift in size distribution. At low permeability (small pore size, 105 μm) particles were equally distributed, except in the small (51–100 μm) category (105 μm, $F_{4,40}$=6.22, P<0.001; Fig. 8A), and Re was 1.4×10^3. During these trials, particles were heavily deposited within 10–20 s of the beginning of each trial. We collected the most particles off the gill rakers during the 105 μm trials; however, there were almost no particles collected in the esophagus (N=30). Particle deposition appeared to occur only on the first three gill slits and the fourth gill slit rarely had many particles. In the 200 μm mesh trials there was a shift in the particle distribution to intermediate to large particles (101–1000 μm; $F_{4,40}$=6.88, P<0.001; Fig. 8B); Re was 2.8×10^3. Again, during these trials almost no particles were collected in the esophagus (N=33 total particles over four replicates) and particle capture was equal across all gill slits. During the 1000 μm mesh trials, capture occurred only along the third and fourth gill slits. Once again primarily large to very large particles were collected (>500 μm; $F_{4,40}$=4.71, P=0.003), although the total distribution of all particle sizes was more uniform compared with the 200 μm mesh trials. We did not collect any particles during the no-mesh trials (Re=2.8×10^5) or the 2000 μm mesh trials (Re=2.5×10^6). Particles collected in all trials were greater in abundance than expected for the large to very large particle sizes (>500 μm) and lower than expected for the small particle sizes (<51 μm). We saw an increase in the proportion of large particles collected compared with the seeding distribution. As expected, the lowest permeability measurements had the highest filtration efficiency of all of the trials (E=1.33‰ for 105 μm and 0.85‰ for 200 μm). The distribution of particles in the 100 μm mesh trials differed significantly from that of the standard model ($F_{4,30}$=7.427, P<0.001) whereas the distribution in the 200 μm trials did not ($F_{4,30}$=1.67, P=0.18). There was a decrease in intermediate particles in the 105 μm trials (~10%) compared with the standard model.

Permeability measurements of the three neonatal whale sharks (mean TL=563±23.8 mm) showed very little extrinsic resistance through their buccal cavities (R=0.91–6.31 Pa ml^{-1} s^{-1}) when flow rate was measured to be constant at 114 ml s^{-1} (Table 2). These resistance measurements were similar to those of other small filter-feeding elasmobranchs (*M. japonica*=0.99 Pa ml^{-1} s^{-1}, *Mobula munkiana* specimen 1=6.36 Pa ml^{-1} s^{-1}, *M. munkiana* specimen 2=2.27 Pa ml^{-1} s^{-1}; Table 2). The calculated pressure head across the filtering apparatus ranged from 106.19 to 171.86 Pa, similar to pressure heads calculated by Motta et al. for adult whale sharks (113 Pa) (Motta et al., 2010).

DISCUSSION

Gill number and swimming speed played major roles in the distribution of particle sizes collected on the gill rakers. This was unexpected as we predicted that the main form of filtration would be dead-end sieving, which should only collect particles larger than the filter pore size. The particles were primarily caught along the gill rakers, which leads us to believe that inertial impaction and gravitational deposition were the prominent filtering mechanisms during these trials, though we cannot rule out the possibility that cyclone filtration was occurring to some degree, as we did document a bilaterally symmetrical vortex near the slits in many of the trials. In several cases we quantified a shift from a bimodal-type filter to an intermediate-type filter or *vice versa*. For example, when we adjusted the number of gill openings from one to five, we saw a shift from a bimodal filter (where primarily 51–100 μm particles and >500 μm particles were filtered) to a filter where only intermediate and large particles were filtered. Surprisingly, we saw this same trend at increased speeds (bimodal distribution to intermediate/large size ranges) except at the five-gill permutation (60 cm s^{-1}), where mostly small particles were caught. This switch to smaller particles collected was unexpected, as higher velocity flow through the oropharyngeal cavity should have increased the contact rate of the most numerous particles in the flow chamber (101–500 μm particles) and, hence, the number of intermediate particles filtered.

Theoretical predictions of an organism's optimized swimming speeds while feeding suggest that the animals should accelerate to maximize the number of prey encountered when feeding in low-density plankton blooms and decelerate when feeding in a high-density plankton bloom (Ware, 1978; Sims, 2000). During the five-gill trial, we observed that the increase in swimming speed also increased the turbulence near the gill openings within the oropharyngeal cavity. More large particles appeared to remain suspended in the turbulent esophageal vortex rather than settling out on the sieve, providing some evidence that the particles may have experienced some degree of cross-flow filtration. This indicates that ram filter feeders, using hydrosol filtration or a combination of inertial impaction and gravitational deposition, should maintain a

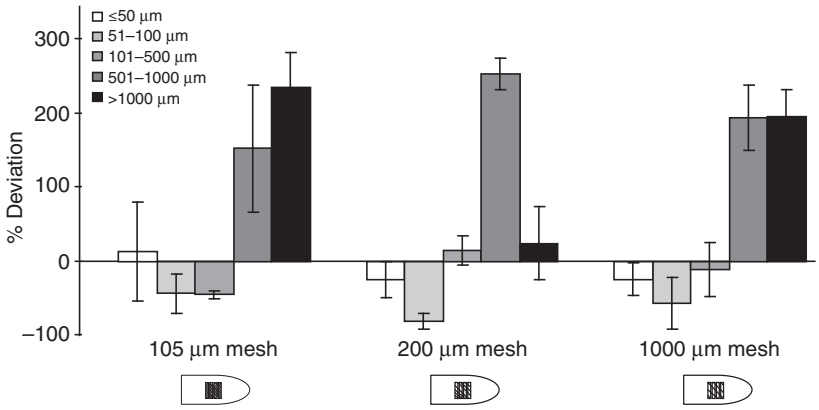

Fig. 8. Percentage deviation from the seeding distribution of particles collected from simulated gill rakers constructed of 105 (N=253, E=1.33‰), 200 (N=261, E=0.85‰) and 1000 μm mesh (N=252, E=0.14‰). We did not collect any particles on 0 or 2000 μm mesh rakers. The filtration efficiency (E) was very high when using small raker sizes (E=27.56‰ for 105 μm and 18.16‰ for 200 μm). Data are means ± s.d.

slower swimming speed regardless of the plankton density if they are targeting larger prey and increase their swimming speed if targeting smaller prey. Organisms primarily utilizing cross-flow or vortex filtration would likely swim at increased speeds to concentrate larger prey in the esophageal vortex prior to swallowing.

Adjustments to the gill morphology resulted in a shift in the particle distributions at the gill rakers from intermediate-type filtration in our control group (501–1000 μm particles collected) to bimodal-type filtration. It is not surprising that increasing the size of the gill slits also resulted in an increased filtering efficiency, as increasing the volume of particle-laden water through this structure should result in increased opportunities for filtration. These large gills would not be necessary in pump suspension- or engulfment-feeding fishes, which filter by first creating a suction force to entrain zooplankton-rich water and then subsequently close their mouths to force this water over the gill rakers. This point is illustrated nicely by comparing the smaller gill morphology of a megamouth shark, *Megachasma pelagios*, which has been hypothesized to use an engulfment feeding strategy (Nakaya et al., 2008), with that of the large-gilled basking sharks (Bigelow and Schroeder, 1953) and whale sharks (Colman, 1997), which use, at least in part, ram suspension feeding. Though we had predicted that ram filtration efficiency would increase with gill size, we did not predict that the particle distribution would shift to that of a planktonic specialist without having to adjust the pore size of the filter. These findings indicate that the morphology of the filter feeder does play a key role in the prey size selectivity of the organism.

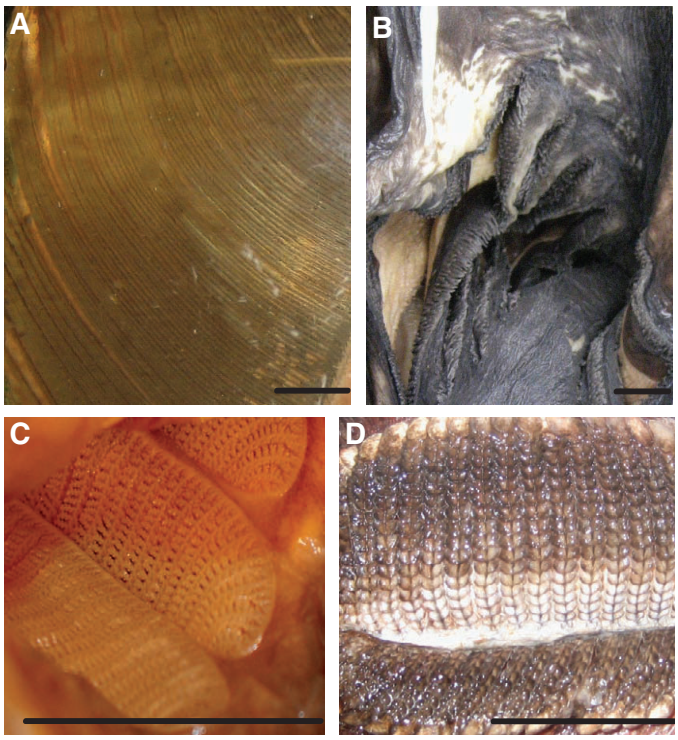

Fig. 9. Gill raker morphology. (A) Basking shark (*Cetorhinus maximus*) rakers extracted from the buccal cavity. (B) Megamouth shark (*Megachasma pelagios*), looking into the buccal cavity through the mouth. (C) Neonatal whale shark (*Rhincodon typus*), looking into the buccal cavity through the mouth. (D) *Mobula* sp., looking at rakers extracted from the buccal cavity. Scale bars, 5 cm (A,B,D) and 4 cm (C).

Perhaps the most obvious parameter affecting captured particle distribution was gill raker permeability, or pore size, which was reflected in our particle distributions. We expected the increased filtration efficiency in decreased pore-size permutations (105 and 200 μm mesh sizes), because the likelihood of a particle contacting the filtering element would be greatly increased relative to the 1000 and 2000 μm mesh sizes. Even with this increase in filtration efficiency at smaller pore size, the greatest mean efficiency we measured was 4.54‰. These seemingly low filtration efficiencies are explained by examining optimal foraging theory (Stephens and Krebs, 1986), which proposes that animals feeding in high-density particle areas can survive well even with low filtration efficiencies, provided that their energetic needs are being met (Shimeta and Jumars, 1991). We would hypothesize that fishes with low filtration efficiencies would likely feed on plankton with high caloric and/or lipid values to meet their energetic needs.

In teleosts, the gill raker structures generally vary by the length of the rakers and their spacing (Nelson, 1967; Bertmar and Strömberg, 1969; Gibson, 1988; Bornbusch and Lee, 1992; van den Berg et al., 1994; Kumari et al., 2005; Friedland et al., 2006; Vigliano et al., 2006). However, the gill raker structures (sometimes referred to as filtering pads) of the filtering cartilaginous fishes exhibit substantial interspecific variation. The four basic raker morphologies are: (1) the bristle-like gill raker structures of the basking shark, *Cetorhinus maximus*; (2) the fur-like short gill rakers of megamouth sharks, *M. pelagios*; (3) the widely spaced, flattened filtering pads of whale sharks, *Rhincodon typus*; and (4) the rigid, leaf-like, folded filtering structure of devil rays and mantas (Mobulidae) (Fig. 9).

These differences in brachial filter morphology among elasmobranchs may result in differences in the basic filtering mechanics (e.g. cross flow, direct interception) and cannot be

addressed using our simplistic mesh morphology. This topic would be best addressed by determining the position of the pad within the buccal cavity and taking an in-depth look at the microstructure of the filtering pad. For example, we cannot evaluate whether a form of hydrosol filtration is occurring without performing histological techniques to determine whether a sufficient number of mucal cells are present. Rubenstein and Koehl noted that the efficiency of a filter can be altered by simply changing the diameter of the pore size or the velocity of the water that passes through it (Rubenstein and Koehl, 1977). Our model's rakers were subjected to high-velocity (45 cm s^{-1}) flow and, when combined with a fine mesh size (105 μm), we predicted that the primary method of particle collection would likely be a form of inertial impaction sieving. As expected, we had the greatest number of particles collected from the gill rakers during this experiment and the particle size was similar across all size ranges. Decreased permeability (smaller pore size) at the gill rakers increased the evenness of the particle sizes that were collected; however, there was no visible evidence that shear flow was moving particles from the mesh to the esophagus. We predict that basking sharks use this type of filtering and would need to either periodically clear the rakers to prevent excessive clogging or continuously transport particles through some mucous-based mechanism. Organisms with a fine mesh size that utilize dead-end sieving (similar to the basking shark) are likely planktonic generalists, feeding on a wide range of particle sizes. As in industrial dead-end sieving, the gill raker structures of organisms using sieve filtration would project into the buccal cavity at a perpendicular orientation to the water flow, resulting in increased filtration efficiency along their surfaces.

The unique morphology of the whale shark's filter pads open up the possibility of cross-flow filtering. In whale sharks, the rakers do not protrude into the buccal cavity. Instead, their morphology suggests that they lay flush with the walls of the epibranchials with sparse spacing (approximately 1000 μm pore size) between each gill raker. In our experiments, the 1000 μm rakers collected large to very large particles. The very small and small particles (<100 μm) did not accumulate, but rather exited easily through the mesh. Adult whale sharks appear to feed primarily through cross-flow filtration (Motta et al., 2010). If neonates are also utilizing some form of cross-flow filtration, we would expect that the majority of the particles collected in the esophagus should be equal to or larger than the pore size of the rakers. With the increased permeability of 2000 μm mesh, there was an increase in the size of particles that were swallowed compared with those swallowed at less permeable pore sizes; however, we could not verify whether cross-flow filtration was occurring.

The model we developed allows us to determine which parameters are important for both dead-end sieving and cross-flow filtration in a way that is difficult to examine using computational models. Empirical data from live ram suspension-feeding fishes is difficult to obtain in teleosts as: (1) they are generally schooling fishes that become agitated when separated from their conspecifics and (2) they are typically small in size, limiting the use of endoscopy (Cheer et al., 2001). Conversely, filter-feeding elasmobranchs are some of the world's largest fishes and are not easily acquired for experimental purposes. Physical models are an inexpensive alternative to maintaining live specimens in a laboratory and can be created by measuring the anatomical parameters of fixed specimens from marine vertebrate collections. By focusing on how the mechanism of filtering changed with differing buccal anatomies, we were able to make predictions about the feeding mechanisms and potential prey preference of suspension-feeding fishes. Our physical model demonstrated that the filtration efficiency and particle size distribution collected during ram suspension feeding is intimately connected to both an individual's anatomy and the swimming speed of the animal.

ACKNOWLEDGEMENTS

This research was supported by NSF Grant IOB–0616322 and by the Alliance for Graduate Education and the Professoriate Competitive Edge Summer Research Program. We would especially like to thank to H. J. Walker and C. Klepadlo at the Scripps Marine Vertebrate Collection for allowing us access to filter-feeding elasmobranchs. Thanks also to T. Kleinteich, S. Crofts and two anonymous reviewers for valuable comments on earlier versions of this manuscript.

REFERENCES

Ballintijn, C. M. (1972). Efficiency, mechanics and motor control of fish respiration. *Respir. Physiol.* **14**, 125-141.
Bertmar, G. and Strömberg, C. (1969). The feeding mechanisms in plankton eaters. The epibranchial organs in whitefish. *Mar. Biol.* **3**, 107-109.
Bigelow, H. B. and Schroeder, W. C. (1953). *Fishes of the Western North Atlantic. Sawfishes, Guitarfishes, Skates and Rays,* Part 2, 514 pp. New Haven, CT: Sears Foundation for Marine Research.
Bornbusch, A. H. and Lee, M. (1992). Gill raker structure and development in Indo-Pacific anchovies (Teleostei: Engrauloidea), with a discussion of the structural evolution of engrauloid gill rakers. *J. Morphol.* **214**, 109-119.
Bott, R., Langeloh, T. H. and Ehrfeld, E. (2000). Dynamic cross flow filtration. *Chem. Eng. J.* **80**, 1-3, 245-249.
Brainerd, E. L. (2001). Caught in the crossflow. *Nature* **412**, 387-388.
Butler, P. J. (1999). Respiratory system. In *Sharks, Skates, and Rays. The Biology of Elasmobranch Fishes* (ed. W. C. Hamlett), pp. 144-173. Baltimore, MD: Johns Hopkins University Press.
Callan, W. T. and Sanderson, S. L. (2003). Feeding mechanisms in carp: crossflow filtration, palatal protrusions and flow reversals. *J. Exp. Biol.* **206**, 883-892.
Cheer, A. Y., Ogami, Y. and Sanderson, S. L. (2001). Computational fluid dynamics in the oral cavity of ram suspension-feeding fishes. *J. Theor. Biol.* **210**, 463-474.
Colman, J. G. (1997). A review of the biology and ecology of the whale shark. *J. Fish Biol.* **51**, 1219-1234.
Dewar, H. (2002). *Preliminary Report: Manta Harvest in Lamakera*, pp. 1-3. Pfleger Institute of Environmental Research.
Dewar, H., Mous, P. and Domeier, M. (2008). Movements and site fidelity of the giant manta ray, *Manta birostris*, in the Komodo Marine Park, Indonesia. *Mar. Biol.* **155**, 121-133.
Drenner, R. W. and Mummert, J. R. (1984). Selective particle ingestion by a filter-feeding fish and its impact on phytoplankton community structure. *Limnol. Oceanogr.* **29**, 941-948.
Friedland, K. D., Ahrenholz, D. W., Smith, J. W., Manning, M. and Ryan, J. (2006). Sieving functional morphology of the gill raker feeding apparatus of Atlantic menhaden. *J. Exp. Zool.* **305A**, 974-985.
Garrido, S., Marcalo, A., Zwolinski, J. and van der Lingen, C. D. (2007). Laboratory investigations on the effect of prey size and concentration on the feeding behaviour of *Sardina pilcharus*. *Mar. Ecol. Prog. Ser.* **330**, 189-199.
Gibson, R. N. (1988). Development, morphometry and particle retention capability of the gill rakers in the herring, *Clupea harengus* L. *J. Fish Biol.* **32**, 949-962.
Goodrich, J., Sanderson, S. A., Batjakas, I. E. and Kaufman, L. S. (2000). Branchial arches of suspension feeding. *Oreochromis esculentus*: sieve or sticky filter? *J. Fish Biol.* **56**, 858-875.
Harder, W. (1975). The digestive tract. In *Anatomy of Fishes*, pp. 135-162. Stuttgart: Eschweizerbartsche Verlagshuchhandlung.
Knutsen, T., Melle, W. and Calise, L. (2001). Determining the mass density of marine copepods and their eggs with a critical focus on some of the previously used methods. *J. Plankton Res.* **23**, 859-873.
Kumari, U., Yashpal, M., Mittal, S. and Mitta, A. K. (2005). Morphology of the pharyngeal cavity, especially the surface ultrastructure of gill arches and gill rakers in relation to the feeding ecology of the catfish *Rita rita* (Siluriformes, Bagridae). *J. Morphol.* **265**, 197-208.
LaBarbera, M. (1984). Feeding currents and particle capture mechanisms in suspension feeding animals. *Am. Zool.* **24**, 71-84.
Langeland, A. and Nøst, T. (1995). Gill raker structure and selective predation on zooplankton by particulate feeding fish. *J. Fish Biol.* **47**, 719-732.
Moloney, C. L. and Field, J. G. (1991). The size-based dynamics of plankton food webs. I. A simulation-model of carbon and nitrogen flows. *J. Plankton Res.* **13**, 1003-1038.
Motta, P. J., Maslanka, M., Hueter, R. E., Davis, R. L., de la Parra, R., Mulvany, S. L., Habegger, M. L., Strother, J. A., Mara, K. R., Gardiner, J. M. et al. (2010). Feeding anatomy, filter-feeding rate, and diet of whale sharks *Rhincodon typus* during surface ram filter-feeding off the Yucatan Peninsula, Mexico. *Zoology* **113**, 199-212.
Nakaya, K., Matsumoto, R. and Suda, K. (2008). Feeding strategy of the megamouth shark *Megachasma pelagios* (Lamniformes:Megachasmidae). *J. Fish Biol.* **73**, 17-34.
Nelson, G. J. (1967). Epibranchial organs in lower teleostean fishes. *J. Zool.* **153**, 71-89.
Piiper, J. and Schumann, D. (1967). Efficiency of O_2 exchange in the gills of the dogfish, *Scyliorhinus stellaris*. *Respir. Physiol.* **2**, 135-148.
Rubenstein, D. I. and Koehl, M. A. R. (1977). The mechanisms of filter-feeding: some theoretical considerations. *Am. Nat.* **111**, 981-994.
Sanderson, S. L., Cech, J. J., and Cheer, A. Y. (1994). Padlefish buccal flow velocity during ram suspension feeding and ram ventilation. *J. Exp. Biol.* **186**, 145-156.

Sanderson, S. L., Cheer, A. Y., Goodrich, J. S., Graziano, J. D. and Callan, W. T. (2001). Crossflow filtration in suspension-feeding fishes. *Nature* **412**, 440-441.
Shimeta, J. and Jumars, P. A. (1991). Physical mechanisms and rates of particle capture by suspension-feeders. *Oceanogr. Mar. Biol. Annu. Rev.* **29**, 191-257.
Sibanda, V., Greenwood, R. W. and Seville, J. P. K. (2001). Particle separation from using cross-flow filtration. *Powder Technol.* **118**, 193-202.
Sims, D. W. (1999). Threshold foraging behaviour of basking sharks on zooplankton: life on an energetic knife-edge? *Proc. R. Soc. Lond. B.* **266**, 1437-1443.
Sims, D. W. (2000). Filter-feeding and cruising swimming speeds of basking sharks compared with optimal models: they filter-feed slower than predicted for their size. *J. Exp. Mar. Biol. Ecol.* **49**, 65-76.
Sims, D. W. and Quayle, V. A. (1998). Selective foraging behaviour of basking sharks on zooplankton in a small-scale front. *Nature* **393**, 460-464.
Skalski, J. R. (1996). Regression of abundance estimates from mark-recapture surveys against environmental covariates. *Can. J. Aquat. Fish. Sci.* **53**, 196-204.
Smith, J. C. and Sanderson, S. L. (2007). Mucus function and crossflow filtration in a fish with gill rakers removed *versus* intact. *J. Exp. Biol.* **210**, 2706-2713.
Stephens, D. W. and Krebs, L. R. (1986). *Foraging Theory*, 247 pp. Princeton, NJ: Princeton University Press.
Stevens, J. D. (2007). Whale shark (*Rhincodon typus*) biology and ecology: a review of the primary literature. *Fish. Res.* **84**, 4-9.
Summers, A. P. and Ferry-Graham, L. A. (2001). Ventilatory modes and mechanics of the hedgehog skate (*Leucoraja erinacea*): testing the continuous flow model. *J. Exp. Biol.* **204**, 1577-1587.
Tanaka, H., Aoki, I. and Ohshimo, S. (2006). Feeding habits and gill raker morphology of three planktivorous pelagic fish species off the coast of northern and western Kyushu in summer. *J. Fish Biol.* **68**, 1041-1061.
Trakumas, S., Willeke, K., Reponen, T., Grinshpun, S. A. and Friedman, W. (2001). Comparison of filter bag, cyclonic, and wet dust collection methods in vacuum cleaners. *AIHA J.* **62**, 573-583.
van den Berg, C., van den Boogaart, J. G. M., Sibbing, F. A. and Osse, J. W. M. (1994). Zooplankton feeding in common bream (*Abramis brama*), white bream (*Blicca bjoerkna*) and roach (*Rutilus rutilus*): experiments, models and energy intake. *Neth. J. Zool.* **44**, 15-42.
van Guelpen, L., Markle, D. F. and Duggen, D. J. (1982). An evaluation of accuracy, precision, and speed of several zooplankton sampling techniques. *J. Cons. Int. Explor. Mer.* **40**, 226-236.
Vigliano, F. A., Aleman, N., Quiroga, M. I. and Nieto, J. M. (2006). Ultrastructural characterization of gills in juveniles of the Argentinean silverside, *Odontesthes bonariensis* (Valenciennes, 1835) (Teleostei: Atheriniformes). *Anat. Histol. Embryol.* **35**, 76-83.
Ware, D. M. (1978). Bioenergetics of pelagic fish: theoretical change in swimming and ration with body size. *J. Fish. Res. Board Can.* **35**, 220-228.